Available online at www.sciencedirect.com
SCIENCE DIRECT®
Journal of Sound and Vibration 280 (2005) 101–125
JOURNAL OF SOUND AND VIBRATION
www.elsevier.com/locate/jsvi

Acoustic scattering from viscoelastically coated spheres and cylinders in viscous fluids

S.M. Hasheminejad*, N. Safari

Department of Mechanical Engineering, Iran University of Science and Technology, Narmak, Tehran 16844, Iran

Received 23 January 2003; accepted 1 December 2003

Abstract

An analysis for sound scattering by simple compound viscoelastic structures immersed in viscous fluids is outlined. The dynamic viscoelastic properties of the scatterer and the viscosity of the surrounding fluid are rigorously taken into account. The Havriliak–Negami model for viscoelastic material behaviour along with the appropriate wave-harmonic field expansions and the pertinent boundary conditions are employed to develop a closed-form solution in form of an infinite series. Subsequently, the associated acoustic field quantities such as the scattered farfield pressure and the form function amplitude are evaluated for given sets of viscoelastic material properties. Numerical results reveal that the scattered farfield pressure directivity patterns are highly dependent on the coating thickness, especially for the low-damping polymeric coating at small and intermediate non-dimensional frequencies. At these frequencies, the high-damping polymeric coating leads to very uniform pressure patterns for essentially all coating thicknesses. Furthermore, numerical solution of the associated eigenfrequency equation confirms that the comparatively high (moderate) scattered farfield pressure amplitudes corresponding to the high-damping (low-damping) polymer at low and intermediate frequencies is due to the fact that the eigenfrequencies associated with the viscoelastic resonances predominantly fall inside this frequency range. Limiting cases are examined and fair agreements with well-known solutions are established.

1. Introduction

Historically, sound wave scattering by cylindrical and spherical objects has been investigated quite extensively since the works of Rayleigh [1] and Lamb [2]. For example, the scattering of acoustic waves has been broadly studied for a rigid, fixed, solid sphere and circular cylinder [3]; for an elastic solid sphere and a circular cylinder [4,5], and for elastic spherical and cylindrical shells [6].

*Corresponding author. Tel.: +98-21-73912936 and 9821-2557166; fax: +98-21-7451143.
E-mail address: hashemi@iust.ac.ir (S.M. Hasheminejad).

0022-460X/$ - see front matter
doi:10.1016/j.jsv.2003.12.027

Junger and Garrelick [7] applied a Kirchhoff-type formulation to compute the backscattering cross-sections of rigid spheres and cylinders covered with partial coatings of arbitrary impedance. Ferri et al. [8] addressed the scattering of acoustic plane waves from submerged objects (cylinders) that are partially covered with a compliant coating. Partridge [9] applied the deformed cylinder method (DCM) to study acoustic scattering from elastic bodies (shells) that are covered to varying degrees by a viscoelastic absorbing layer. Honarvar and Sinclair [10] developed a detailed formulation for the scattering of an obliquely incident plane acoustic wave from a submerged clad rod. Roumeliotis and Kakogiannos [11] treated the scattering of a plane acoustic wave normal to the axis of an infinite impenetrable or penetrable cylinder of acoustically small radius, coated by a penetrable cylinder. The latter authors also studied the scattering of a plane acoustic wave from an impenetrable or a penetrable sphere of acoustically small radius coated by another penetrable sphere [12]. Similarly, in a series of articles, the problems of low-frequency scattering of a point source field by a soft or a hard small sphere with a lossy coating [13], by a coated sphere with a resistive core [14], and by a penetrable lossy sphere with a lossy coating [15] have been treated.

Investigations of sound scattering by various objects with allowance for various dissipation mechanisms, such as viscous and thermal losses and complicated boundary or scatterer models, have been reported in a great many papers [16,17]. The sustained interest in these problems is due to the importance of scattering and attenuation in many areas of research such as cloud physics, rocket propulsion, dispersion ultrasonics and underwater acoustics. The inclusion of viscosity in the fluid model was first made by Sewell [18], who treated sound absorption by rigid, fixed spheres and circular cylinders in a viscous gas. Later, Lamb [2] simplified Sewell's treatment and studied sound scattering by rigid, fixed or movable spheres in a viscous fluid. Lin and Raptis [19] presented analytical solutions as well as numerical results for the boundary value problem concerning the interaction of a plane sound wave with elastic solid cylinders and spheres immersed in viscous fluids. They studied the effects of the fluid viscosity and scatterer's elasticity on acoustic-wave scattering patterns and acoustic-radiation force. Subsequently, the same authors presented a general analysis for scattering of a plane sound wave obliquely incident upon a thin, elastic circular cylinder (rod) immersed in an unbounded viscous fluid [20]. Hasegawa and Watanabe [21] modified the standard harmonic series theory to study the effect of hysteresis type of absorption on the acoustic field of an absorbing sphere immersed in an ideal fluid. Their analysis, however, is applicable to materials with frequency-independent sound absorption per wavelength and may not be considered to be satisfactory from the standpoint of generality and completeness. Just recently, Hasheminejad and Harsini [22] employed the novel features of Havriliak–Negami (HN) model to investigate effects of dynamic viscoelastic properties on acoustic scattering by a solid sphere submerged in a viscous fluid. Their numerical results revealed a generally lower (higher) level of scattered field directionality for the scatterer with a higher (lower) degree of viscoelasticity (damping). The prime objective of the present work is to use HN theory to investigate acoustic interaction of sound waves with viscoelastically coated spheres and cylinders. The proposed analysis is of particular interest in every practical application in which the frequency (body dimension) is so low (small) that the viscous boundary layer effects become consequential (i.e., the body dimension is comparable to the viscous boundary layer in the surrounding fluid [19,20,22]). For example, it can be useful for ultrasonic characterization of polymer-coated colloidal particles (dispersions) [23,24]. It can also provide a valuable model for nondestructive evaluation (NDE) and on-line monitoring of the physical properties (material

characterization) of various cylindrical components such as polymer-clad thin metallic rods (wires) using resonance acoustic spectroscopy (RAS) techniques [25].

2. Viscoelastic model

Accurate mathematical modelling of viscoelastic materials is difficult mainly because their measured dynamic properties are frequency and temperature dependent, and can also depend on the type of deformation and amplitude. Consequently, mathematical models describing the behaviour of viscoelastic materials cannot be clearly linked to the physical principles involved and thus empirical approaches are used. The most popular approach, called the structural damping model, uses complex constants as the material moduli. Strictly speaking, for viscoelastic and isotropic materials, two independent complex moduli are necessary for mechanical characterization; for example the Young's modulus $E^*(\omega) = E'(\omega) + iE''(\omega)$ and the shear modulus $G^*(\omega) = G'(\omega) + iG''(\omega)$. Both moduli, in principle, are frequency dependent. The main difficulty is the simultaneous presence of the Young's and shear complex moduli as well as the Poisson ratio. Practically, however, for viscoelastic isotropic materials the hypothesis of a constant (frequency independent) and real Poisson ratio is often adopted [26]. This assumption has been validated with some experiments [27], revealing that the imaginary part of the Poisson ratio of elastomers is less than 1% of the real part.

Frequency dependence of $G'(\omega)$ and $G''(\omega)$ in the viscoelastic transition region has been the object of many experimental and theoretical studies [28]. The most successful description for the frequency dependence of the complex modulus of polymers in the glass transition region is perhaps given by Havriliak–Negami model [29]. According to HN model, the real and imaginary parts of the complex modulus are given by [30]

$$G'(\omega) = G_\infty + \frac{(G_0 - G_\infty)\cos(\beta\kappa)}{[1 + 2\omega^\alpha\tau^\alpha\cos\gamma + \omega^{2\alpha}\tau^{2\alpha}]^{\beta/2}}, \tag{1a}$$

$$G''(\omega) = \frac{(G_\infty - G_0)\sin(\beta\kappa)}{[1 + 2\omega^\alpha\tau^\alpha\cos\gamma + \omega^{2\alpha}\tau^{2\alpha}]^{\beta/2}}, \tag{1b}$$

where $\gamma = \alpha\pi/2$, and the loss factor is specified by

$$\eta(\omega) = \frac{G''(\omega)}{G'(\omega)} = \frac{(1-\chi)\sin(\beta\kappa)}{[1 + 2\omega^\alpha\tau^\alpha\cos\gamma + \omega^{2\alpha}\tau^{2\alpha}]^{\beta/2} - (1-\chi)\cos(\beta\kappa)} \tag{2}$$

in which $\chi = G_0/G_\infty$, and

$$\kappa(\omega) = \tan^{-1}\frac{\omega^\alpha\tau^\alpha\sin\gamma}{1 + \omega^\alpha\tau^\alpha\cos\gamma}. \tag{3}$$

Note that $\eta(\omega)$ depends only on the ratio $\chi = G_0/G_\infty$ and not on their individual values. Furthermore, G_0 (relaxed modulus) and G_∞ (unrelaxed modulus) are the limiting values of the shear modulus at low and high frequencies, respectively, $\tau(= 1/\omega_0)$ is the relaxation time associated with the polymer glass transition centre frequency (loss factor peak), α is a dimensionless parameter $(0<\alpha<1)$ that governs the width of the relaxation, and β is another dimensionless parameter $(0<\beta<1)$ that governs the asymmetry of the relaxation.

3. Governing field equations

Following the standard methods of continuum mechanics, the linearized equations of continuity and Navier–Stokes for a viscous non-heat-conducting compressible fluid are, respectively [31],

$$\frac{\partial \rho}{\partial t} + \rho \nabla \cdot \mathbf{u} = 0, \tag{4a}$$

$$\rho \frac{\partial \mathbf{u}}{\partial t} + \nabla p = \mu \nabla^2 \mathbf{u} + \left(\tfrac{1}{3}\mu + \mu_b\right) \nabla(\nabla \cdot \mathbf{u}). \tag{4b}$$

Here, ρ is the total mass density, p represents the deviation of pressure from its mean value, $\mathbf{u}$ is the fluid velocity, and μ and μ_b are the shear and the expansive (bulk) coefficient of viscosity, respectively. For a barotropic fluid, the linearized equation of state is $p = c^2 \rho'$, where, as usual, c is the ideal speed of sound evaluated at ambient conditions and ρ' is the deviation of density from equilibrium (i.e., the time-varying part of the density). Eqs. (4) can readily be combined to yield a single equation for the velocity vector $\mathbf{u}$:

$$\frac{\partial^2 \mathbf{u}}{\partial t^2} - c^2 \nabla(\nabla \cdot \mathbf{u}) = \frac{\mu}{\rho} \nabla^2 \frac{\partial \mathbf{u}}{\partial t} + \frac{1}{\rho}\left(\tfrac{1}{3}\mu + \mu_b\right) \nabla\left(\nabla \cdot \frac{\partial \mathbf{u}}{\partial t}\right). \tag{5}$$

The Helmholtz decomposition theorem allows one to resolve the velocity fields as the superposition of longitudinal and transverse vector components

$$\mathbf{u} = -\nabla \varphi + \nabla \times \boldsymbol{\psi}. \tag{6}$$

Introducing the above decomposition into Eq. (5), making use of problem symmetry, $\boldsymbol{\psi} = (0., 0., \psi)$, and the calibration condition, $\nabla \cdot \boldsymbol{\psi} = 0$, a set of two equations is deduced

$$\frac{\partial^2 \varphi}{\partial t^2} = \left[c^2 + \frac{1}{\rho}\left(\tfrac{4}{3}\mu + \mu_b\right)\frac{\partial}{\partial t}\right] \nabla^2 \varphi, \tag{7a}$$

$$\frac{\partial \psi}{\partial t} = \frac{\mu}{\rho} \nabla^2 \psi. \tag{7b}$$

If the incident wave is assumed to be monochromatic, one expects solutions of the form

$$\varphi(r, \theta, t) = Re[\varphi(r, \theta, \omega) \mathrm{e}^{-\mathrm{i}\omega t}], \tag{8a}$$

$$\psi(r, \theta, t) = Re[\psi(r, \theta, \omega) \mathrm{e}^{-\mathrm{i}\omega t}], \tag{8b}$$

where *Re* indicates the real part of a complex number, and quantities $\varphi(r, \theta, \omega)$ and $\psi(r, \theta, \omega)$ may be complex. Incorporation of above assumptions in Eqs. (7), after some manipulations, yields

$$(\nabla^2 + k_c^2)\varphi = 0, \tag{9a}$$

$$(\nabla^2 + k_s^2)\psi = 0, \tag{9b}$$

where the complex compressional and shear wave numbers in the viscous fluid are given by [31]

$$k_c = \frac{\omega}{c}\left(1 + \mathrm{i}\frac{\omega\mu}{2\rho c^2}\left(\tfrac{4}{3} + \frac{\mu_b}{\mu}\right)\right), \tag{10a}$$

$$k_s = (1+\mathrm{i})\sqrt{\frac{\omega\rho}{2\mu}}. \tag{10b}$$

The viscoelastic material under consideration is assumed to be linear, macroscopically homogeneous, and isotropic for which the constitutive equation, for harmonic time functions, may be written as [32]

$$\sigma_{ij} = \lambda^*(\omega)\delta_{ij}\varepsilon_{kk} + 2\mu_s^*(\omega)\varepsilon_{ij}, \tag{11}$$

where δ_{ij} is Kronecker delta symbol, $\lambda^*(\omega)$ and $\mu_s^*(\omega)$ are complex, frequency-dependent Lame functions which are determined according to the standard relations

$$\lambda^*(\omega) = \frac{2v}{(1-2v)}G^*(\omega), \tag{12a}$$

$$\mu_s^*(\omega) = G^*(\omega) \tag{12b}$$

in which the real and imaginary parts of the complex shear modulus, $G^*(\omega)$, are specified in Eqs. (1). The wave motion inside the viscoelastic scatterer is governed by the classical Navier's equation [33]

$$\rho_s \frac{\partial^2 \mathbf{U}}{\partial t^2} = \mu_s^* \nabla^2 \mathbf{U} + (\lambda^* + \mu_s^*)\nabla(\nabla \cdot \mathbf{U}) \tag{13}$$

subject to the appropriate boundary conditions. Here, ρ_s is the solid material density, and $\mathbf{U}$ is the vector displacement that can advantageously be expressed as sum of the gradient of a scalar potential and the curl of a vector potential

$$\mathbf{U} = \nabla\Phi + \nabla \times \mathbf{\Psi} \tag{14}$$

with the condition $\nabla \cdot \mathbf{\Psi} = 0$, and $\mathbf{\Psi} = (0., 0., \Psi)$. The above decomposition enables one to separate the dynamic equation of motion into the classical Helmholtz equations:

$$(\nabla^2 + K_c^{*2})\Phi = 0, \tag{15a}$$

$$(\nabla^2 + K_s^{*2})\Psi = 0, \tag{15b}$$

where K_c^* and K_s^* are complex wave numbers, known as [32]

$$K_c^* = \frac{\omega}{\sqrt{[\lambda^*(\omega) + 2\mu_s^*(\omega)]/\rho_s}}, \tag{16a}$$

$$K_s^* = \frac{\omega}{\sqrt{\mu_s^*(\omega)/\rho_s}}. \tag{16b}$$

4. Scattering of sound waves by a compound sphere

In this section, the general problem of acoustic scattering from a compound viscoelastic sphere suspended in an unbounded viscous fluid is considered. The geometry and the co-ordinate system used are depicted in Fig. 1a. Mathematically, the dynamics of the problem may be expressed in

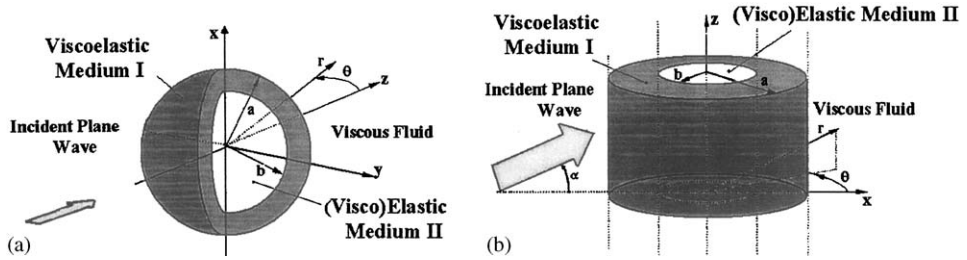

Fig. 1. Problem geometry: (a) spherical co-ordinate system; (b) cylindrical co-ordinate system.

terms of appropriate scalar and vector potentials. The expansion of the incident plane wave in spherical co-ordinate has the form [34]

$$\varphi_{inc.}(r,\theta) = \phi_0 \sum_{n=0}^{\infty} (2n+1)\mathrm{i}^n \mathrm{j}_n(k_c r) P_n(\cos\theta), \tag{17}$$

where j_n are spherical Bessel functions [35], P_n are Legendre polynomials, and ϕ_0 is the amplitude of the incident wave. Likewise, noting that the fluid medium is unbounded and keeping in mind the radiation condition, the solutions of the Helmholtz equations for the potentials can be expressed as a linear combination of outgoing spherical waves:

$$\varphi_c(r,\theta) = \sum_{n=0}^{\infty} (2n+1)\mathrm{i}^n A_n h_n^{(1)}(k_c r) P_n(\cos\theta), \tag{18a}$$

$$\psi(r,\theta) = \sum_{n=1}^{\infty} (2n+1)\mathrm{i}^n B_n h_n^{(1)}(k_s r) P_n^1(\cos\theta), \tag{18b}$$

where $h_n^{(1)}$ are spherical Hankel functions of first kind [35], $P_n^1 = -(\mathrm{d}/\mathrm{d}\theta)P_n$ are associated Legendre functions, and A_n and B_n are unknown scattering coefficients. Similarly, the longitudinal and transverse waves in the viscoelastic coating are represented by

$$\Phi_1(r,\theta) = \sum_{n=0}^{\infty} (2n+1)\mathrm{i}^n \left[C_n h_n^{(1)}(K_{c1}^* r) + D_n h_n^{(2)}(K_{c1}^* r)\right] P_n(\cos\theta), \tag{19a}$$

$$\Psi_1(r,\theta) = \sum_{n=1}^{\infty} (2n+1)\mathrm{i}^n \left[E_n h_n^{(1)}(K_{s1}^* r) + F_n h_n^{(2)}(K_{s1}^* r)\right] P_n^1(\cos\theta), \tag{19b}$$

where $h_n^{(2)}$ are spherical Hankel functions of second kind [35], and the corresponding waves in the core medium are

$$\Phi_2(r,\theta) = \sum_{n=0}^{\infty} (2n+1)\mathrm{i}^n G_n \mathrm{j}_n(K_{c2}^* r) P_n(\cos\theta), \tag{20a}$$

$$\Psi_2(r,\theta) = \sum_{n=1}^{\infty} (2n+1)\mathrm{i}^n Q_n \mathrm{j}_n(K_{s2}^* r) P_n^1(\cos\theta), \tag{20b}$$

where the subscripts 1 and 2 refer to medium I (coating) and medium II (core), respectively, and the superscript * indicates that complex, frequency-dependent viscoelastic properties are involved.

Now considering the basic field equations in spherical co-ordinates, the velocity components of the waves in r- and θ-directions in terms of potentials in the viscous fluid are [31]

$$u_r = -\frac{\partial\varphi}{\partial r} + \frac{1}{r\sin\theta}\frac{\partial(\psi\sin\theta)}{\partial\theta}, \tag{21a}$$

$$u_\theta = -\frac{1}{r}\frac{\partial\varphi}{\partial\theta} - \frac{1}{r}\frac{\partial(r\psi)}{\partial r}, \tag{21b}$$

where $\varphi = \varphi_{inc.} + \varphi_c$. Similarly, the displacements in the viscoelastic scatterer are [33]

$$\begin{aligned} U_r^{s1} &= \frac{\partial\Phi_1}{\partial r} + \frac{1}{r\sin\theta}\frac{\partial(\Psi_1\sin\theta)}{\partial\theta}, \quad U_r^{s2} = \frac{\partial\Phi_2}{\partial r} + \frac{1}{r\sin\theta}\frac{\partial(\Psi_2\sin\theta)}{\partial\theta}, \\ U_\theta^{s1} &= \frac{1}{r}\frac{\partial\Phi_1}{\partial\theta} - \frac{1}{r}\frac{\partial(r\Psi_1)}{\partial r}, \quad U_\theta^{s2} = \frac{1}{r}\frac{\partial\Phi_2}{\partial\theta} - \frac{1}{r}\frac{\partial(r\Psi_2)}{\partial r}. \end{aligned} \tag{22}$$

The stress components in the viscous fluid are [31]

$$\sigma_{rr} = -p + (\mu_b - \tfrac{2}{3}\mu)\Delta + 2\mu(\partial u_r/\partial r) \tag{23a}$$

$$\sigma_{r\theta} = \mu\left(\frac{1}{r}\frac{\partial u_r}{\partial\theta} + \frac{\partial u_\theta}{\partial r} - \frac{u_\theta}{r}\right) \tag{23b}$$

where

$$p = -\mathrm{i}\omega\rho\varphi + (\mu_b + \tfrac{4}{3}\mu)\Delta \tag{24}$$

in which $\Delta = \nabla\cdot\mathbf{u} = -\nabla^2\varphi = k_c^2\varphi$. The stresses in the viscoelastic scatterer are [33]

$$\begin{aligned} \sigma_{rr}^{s1} &= 2\mu_{s1}^*\frac{\partial U_r^{s1}}{\partial r} + \lambda_1^*\varepsilon_1, \quad \sigma_{rr}^{s2} = 2\mu_{s2}^*\frac{\partial U_r^{s2}}{\partial r} + \lambda_2^*\varepsilon_2, \\ \sigma_{r\theta}^{s1} &= \mu_{s1}^*\left(\frac{1}{r}\frac{\partial U_r^{s1}}{\partial\theta} + \frac{\partial U_\theta^{s1}}{\partial r} - \frac{U_\theta^{s1}}{r}\right), \quad \sigma_{r\theta}^{s2} = \mu_{s2}^*\left(\frac{1}{r}\frac{\partial U_r^{s2}}{\partial\theta} + \frac{\partial U_\theta^{s2}}{\partial r} - \frac{U_\theta^{s2}}{r}\right), \end{aligned} \tag{25}$$

where $\varepsilon_1 = \nabla\cdot\mathbf{U}_{s1} = \nabla^2\Phi_1 = -K_{c1}^{*2}\Phi_1$, and $\varepsilon_2 = \nabla\cdot\mathbf{U}_{s2} = \nabla^2\Phi_2 = -K_{c2}^{*2}\Phi_2$.

The appropriate boundary conditions that must hold at the interfaces of the core material with the coating, and the coating with the viscous fluid medium are continuity of velocity and stress components, i.e.,

$$\begin{aligned} &u_r(r,\theta,\omega)]_{r=a} = -\mathrm{i}\omega U_r^{s1}(r,\theta,\omega)]_{r=a}, \quad U_r^{s1}(r,\theta,\omega)]_{r=b} = U_r^{s2}(r,\theta,\omega)]_{r=b}, \\ &u_\theta(r,\theta,\omega)]_{r=a} = -\mathrm{i}\omega U_\theta^{s1}(r,\theta,\omega)]_{r=a}, \quad U_\theta^{s1}(r,\theta,\omega)]_{r=b} = U_\theta^{s2}(r,\theta,\omega)]_{r=b}, \\ &\sigma_{rr}(r,\theta,\omega)]_{r=a} = \sigma_{rr}^{s1}(r,\theta,\omega)]_{r=a}, \quad \sigma_{rr}^{s1}(r,\theta,\omega)]_{r=b} = \sigma_{rr}^{s2}(r,\theta,\omega)]_{r=b}, \\ &\sigma_{r\theta}(r,\theta,\omega)]_{r=a} = \sigma_{r\theta}^{s1}(r,\theta,\omega)]_{r=a}, \quad \sigma_{r\theta}^{s1}(r,\theta,\omega)]_{r=b} = \sigma_{r\theta}^{s2}(r,\theta,\omega)]_{r=b}. \end{aligned} \tag{26}$$

The unknown scattering coefficients shall be determined by imposing the stated boundary conditions. Employing expansions (17)–(20) in the field equations (21)–(25), and substituting the obtained results into the boundary conditions (26), one obtains, for the nth mode

$$-k_c A_n h_n^{(1)'}(k_c a)+\frac{n(n+1)}{a}B_n h_n^{(1)}(k_s a)+\mathrm{i}\omega K_{c1}^*[C_n h_n^{(1)'}(K_{c1}^* a)+D_n h_n^{(2)'}(K_{c1}^* a)] + \mathrm{i}\omega\frac{n(n+1)}{a}[E_n h_n^{(1)}(K_{s1}^* a)+F_n h_n^{(2)}(K_{s1}^* a)]=k_c\phi_0 \mathrm{j}_n'(k_c a), \tag{27a}$$

$$A_n h_n^{(1)}(k_c a)-[h_n^{(1)}(k_s a)+k_s a h_n^{(1)'}(k_s a)]B_n-\mathrm{i}\omega[C_n h_n^{(1)}(K_{c1}^* a)+D_n h_n^{(2)}(K_{c1}^* a)] -\mathrm{i}\omega\{[h_n^{(1)}(K_{s1}^* a)+k_{s1}^* a h_n^{(1)'}(K_{s1}^* a)]E_n+[h_n^{(2)}(K_{s1}^* a)+K_{s1}^* a h_n^{(2)'}(K_{s1}^* a)]F_n\} =-\phi_0 \mathrm{j}_n(k_c a), \tag{27b}$$

$$[(\mathrm{i}\omega\rho-2\mu k_c^2)h_n^{(1)}(k_c a)-2\mu k_c^2 h_n^{(1)''}(k_c a)]A_n-\frac{2\mu n(n+1)}{a^2}[h_n^{(1)}(k_s a)-k_s a h_n^{(1)'}(k_s a)]B_n - K_{c1}^{*2}\{[2\mu_{s1}^* h_n^{(1)''}(K_{c1}^* a)-\lambda_1^* h_n^{(1)}(K_{c1}^* a)]C_n+[2\mu_{s1}^* h_n^{(2)''}(K_{c1}^* a)-\lambda_1^* h_n^{(2)}(K_{c1}^* a)]D_n\} +\frac{2\mu_{s1}^* n(n+1)}{a^2}\{[h_n^{(1)}(K_{s1}^* a)-K_{s1}^* a h_n^{(1)'}(K_{s1}^* a)]E_n+[h_n^{(2)}(K_{s1}^* a)-K_{s1}^* a h_n^{(2)'}(K_{s1}^* a)]F_n\} =-[(\mathrm{i}\omega\rho-2\mu k_c^2)\mathrm{j}_n(k_c a)-2\mu k_c^2 \mathrm{j}_n''(k_c a)]\phi_0, \tag{27c}$$

$$-2\mu[h_n^{(1)}(k_c a)-k_c a h_n^{(1)'}(k_c a)]A_n+\mu\{[2-n(n+1)]h_n^{(1)}(k_s a)-k_s^2 a^2 h_n^{(1)''}(k_s a)\}B_n + 2\mu_{s1}^*\{[K_{c1}^* a h_n^{(1)'}(K_{c1}^* a)-h_n^{(1)}(K_{c1}^* a)]C_n+[K_{c1}^* a h_n^{(2)'}(K_{c1}^* a)-h_n^{(2)}(K_{c1}^* a)]D_n\} - \mu_{s1}^*\{[2-n(n+1)]h_n^{(1)}(K_{s1}^* a)-K_{s1}^{*2} a^2 h_n^{(1)''}(K_{s1}^* a)\}E_n-\mu_{s1}^*\{[2-n(n+1)]h_n^{(2)}(K_{s1}^* a) - K_{s1}^{*2} a^2 h_n^{(2)''}(K_{s1}^* a)\}F_n=2\mu[\mathrm{j}_n(k_c a)-k_c a \mathrm{j}_n'(k_c a)]\phi_0, \tag{27d}$$

$$-K_{c1}^*[C_n h_n^{(1)'}(K_{c1}^* b)+D_n h_n^{(2)'}(K_{c1}^* b)]-\frac{n(n+1)}{b}[E_n h_n^{(1)}(K_{s1}^* b)+F_n h_n^{(2)}(K_{s1}^* b)] + K_{c2}^* \mathrm{j}_n'(K_{c2}^* b)G_n+\frac{n(n+1)}{b}Q_n \mathrm{j}_n(K_{s2}^*)=0, \tag{27e}$$

$$C_n h_n^{(1)}(K_{c1}^* b)+D_n h_n^{(2)}(K_{c1}^* b)+[h_n^{(1)}(K_{s1}^* b)+K_{s1}^* b h_n^{(1)'}(K_{s1}^* b)]E_n+[h_n^{(2)}(K_{s1}^* b) + K_{s1}^* b h_n^{(2)'}(K_{s1}^* b)]F_n-G_n \mathrm{j}_n(K_{c2}^* b)-[\mathrm{j}_n(K_{s2}^* b)+K_{s2}^* b \mathrm{j}_n'(K_{s2}^* b)]Q_n=0, \tag{27f}$$

$$K_{c1}^{*2}\{[\lambda_1^* h_n^{(1)}(K_{c1}^* b)-2\mu_{s1}^* h_n^{(1)''}(K_{c1}^* b)]C_n+[\lambda_1^* h_n^{(2)}(K_{c1}^* b)-2\mu_{s1}^* h_n^{(2)''}(K_{c1}^* b)]D_n\} -\frac{2n(n+1)}{b^2}\mu_{s1}^*\{[-h_n^{(1)}(K_{s1}^* b)+K_{s1}^* b h_n^{(1)'}(K_{s1}^* b)]E_n + [-h_n^{(2)}(K_{s1}^* b)+K_{s1}^* b h_n^{(2)'}(K_{s1}^* b)]F_n\}+K_{c2}^{*2}[2\mu_{s2}^* \mathrm{j}_n''(K_{c2}^* b)-\lambda_2^* \mathrm{j}_n(K_{c2}^* b)]G_n - \frac{2\mu_{s2}^* n(n+1)}{b^2}[\mathrm{j}_n(K_{s2}^* b)-K_{s2}^* b \mathrm{j}_n'(K_{s2}^* b)]Q_n=0, \tag{27g}$$

$$
\begin{aligned}
&2\mu_{s1}^{*}[K_{c1}^{*}bh_n^{(1)'}(K_{c1}^{*}b)-h_n^{(1)}(K_{c1}^{*}b)]C_n+2\mu_{s1}^{*}[K_{c1}^{*}bh_n^{(2)'}(K_{c1}^{*}b)-h_n^{(2)}(K_{c1}^{*}b)]D_n\\
&\quad-\mu_{s1}^{*}\{[2-n(n+1)]h_n^{(1)}(K_{s1}^{*}b)-K_{s1}^{*2}b^2h_n^{(1)''}(K_{s1}^{*}b)\}E_n\\
&\quad-\mu_{s1}^{*}\{[2-n(n+1)]h_n^{(2)}(K_{s1}^{*}b)-K_{s1}^{*2}b^2h_n^{(2)''}(K_{s1}^{*}b)\}F_n\\
&\quad-2\mu_{s2}^{*}[K_{c2}^{*}b\mathrm{j}_n'(K_{c2}^{*}b)-\mathrm{j}_n(K_{c2}^{*}b)]G_n\\
&\quad+\mu_{s2}^{*}[[2-n(n+1)]\mathrm{j}_n(K_{s2}^{*}b)-K_{s2}^{*2}\mathrm{j}_n''(K_{s2}^{*}b)]Q_n=0,
\end{aligned}
\tag{27h}
$$

where $n=0,1,2,\ldots$, except for Eqs. (27b,d,f,h) where $n=1,2,\ldots$.

5. Scattering of sound waves by a compound cylinder

Here, a compressional planar monochromatic sound wave of angular frequency ω obliquely incident upon a compound viscoelastic cylinder immersed in an unbounded viscous fluid at rest (Fig. 1b) is considered. The dynamics of the problem may be expressed in terms of appropriate scalar potentials. First, the expansion of the incident plane wave in cylindrical co-ordinate has the form [34]

$$
\varphi_{inc.}=\phi_0\sum_{n=0}^{\infty}\varepsilon_n\mathrm{i}^n\mathrm{J}_n(\gamma_c r)\cos n\theta\mathrm{e}^{\mathrm{i}k_z z},
\tag{28}
$$

where $\varepsilon_0=1$, and $\varepsilon_n=2$ for $n>0$, ϕ_0 is the amplitude of the incident wave, J_n are cylindrical Bessel functions of first kind [35], and $\gamma_c=\sqrt{k_c^2-k_z^2}$ in which $k_z=Re(k_c\sin\alpha)$ where α is the angle of plane wave incidence. Second, noting that the fluid medium is unbounded and keeping in mind the radiation condition, the solution can be expressed as a linear combination of outgoing cylindrical waves as follows:

$$
\begin{aligned}
&\varphi_c=\sum_{n=0}^{\infty}A_nH_n^{(1)}(\gamma_c r)\cos n\theta\mathrm{e}^{\mathrm{i}k_z z},\quad \psi_\theta=-\sum_{n=0}^{\infty}B_nH_{n+1}^{(1)}(\gamma_s r)\cos n\theta\mathrm{e}^{\mathrm{i}k_z z},\\
&\psi_r=\sum_{n=1}^{\infty}B_nH_{n+1}^{(1)}(\gamma_s r)\sin n\theta\mathrm{e}^{\mathrm{i}k_z z},\quad \psi_z=\sum_{n=1}^{\infty}C_nH_n^{(1)}(\gamma_s r)\sin n\theta\mathrm{e}^{\mathrm{i}k_z z},
\end{aligned}
\tag{29}
$$

where $H_n^{(1)}$ are cylindrical Hankel functions of first kind [35], A_n, B_n and C_n are unknown scattering coefficients, and $\gamma_s=\sqrt{k_s^2-k_z^2}$. Third, the longitudinal and transverse waves in the viscoelastic coating (medium I) are represented by

$$
\begin{aligned}
&\Phi^{(1)}=\sum_{n=0}^{\infty}[D_nH_n^{(1)}(\Gamma_{c1}r)+E_nH_n^{(2)}(\Gamma_{c1}r)]\cos n\theta\mathrm{e}^{\mathrm{i}k_z z},\\
&\Psi_r^{(1)}=\sum_{n=1}^{\infty}[F_nH_{n+1}^{(1)}(\Gamma_{s1}r)+G_nH_{n+1}^{(2)}(\Gamma_{s1}r)]\sin n\theta\mathrm{e}^{\mathrm{i}k_z z},
\end{aligned}
$$

$$\Psi_\theta^{(1)} = -\sum_{n=0}^{\infty} [F_n H_{n+1}^{(1)}(\Gamma_{s1} r) + G_n H_{n+1}^{(2)}(\Gamma_{s1} r)] \cos n\theta e^{ik_z z},$$

$$\Psi_z^{(1)} = \sum_{n=1}^{\infty} [K_n H_n^{(1)}(\Gamma_{s1} r) + L_n H_n^{(2)}(\Gamma_{s1} r)] \sin n\theta e^{ik_z z}, \tag{30}$$

where $H_n^{(2)}$ are cylindrical Hankel functions of second kind [35], and $\Gamma_{c1} = \sqrt{K_{c1}^{*2} - k_z^2}$, $\Gamma_{s1} = \sqrt{K_{s1}^{*2} - k_z^2}$. Furthermore, the transmitted waves in the core (medium II) are

$$\Phi^{(2)} = \sum_{n=0}^{\infty} M_n \mathrm{J}_n(\Gamma_{c2} r) \cos n\theta e^{ik_z z}, \quad \Psi_\theta^{(2)} = -\sum_{n=0}^{\infty} N_n \mathrm{J}_{n+1}(\Gamma_{s2} r) \cos n\theta e^{ik_z z},$$

$$\Psi_r^{(2)} = \sum_{n=1}^{\infty} N_n \mathrm{J}_{n+1}(\Gamma_{s2} r) \sin n\theta e^{ik_z z}, \quad \Psi_z^{(2)} = \sum_{n=1}^{\infty} Q_n \mathrm{J}_n(\Gamma_{s2} r) \sin n\theta e^{ik_z z}, \tag{31}$$

where $\Gamma_{c2} = \sqrt{K_{c2}^{*2} - k_z^2}$ and $\Gamma_{s2} = \sqrt{K_{s2}^{*2} - k_z^2}$.

Now considering the basic field equations in cylindrical co-ordinates, the velocity components of the waves in r- and θ-directions in terms of potentials in the viscous fluid are [19]

$$u_r = -\frac{\partial \varphi}{\partial r} + \frac{1}{r}\frac{\partial \psi_z}{\partial \theta} - \frac{\partial \psi_\theta}{\partial z}, \tag{32a}$$

$$u_\theta = -\frac{1}{r}\frac{\partial \varphi}{\partial \theta} + \frac{\partial \psi_r}{\partial z} - \frac{\partial \psi_z}{\partial r}, \tag{32b}$$

$$u_z = -\frac{\partial \varphi}{\partial z} + \frac{1}{r}\frac{\partial (r\psi_\theta)}{\partial r} - \frac{1}{r}\frac{\partial \psi_r}{\partial \theta}, \tag{32c}$$

where $\varphi = \varphi_{inc.} + \varphi_c$. Similarly, the relevant displacements in the viscoelastic scatterer are [33]

$$U_r^{s1} = \frac{\partial \Phi^{(1)}}{\partial r} + \frac{1}{r}\frac{\partial \Psi_z^{(1)}}{\partial \theta} - \frac{\partial \Psi_\theta^{(1)}}{\partial z}, \quad U_r^{s2} = \frac{\partial \Phi^{(2)}}{\partial r} + \frac{1}{r}\frac{\partial \Psi_z^{(2)}}{\partial \theta} - \frac{\partial \Psi_\theta^{(2)}}{\partial z},$$

$$U_\theta^{s1} = \frac{1}{r}\frac{\partial \Phi^{(1)}}{\partial \theta} + \frac{\partial \Psi_r^{(1)}}{\partial z} - \frac{\partial \Psi_z^{(1)}}{\partial r}, \quad U_\theta^{s2} = \frac{1}{r}\frac{\partial \Phi^{(2)}}{\partial \theta} + \frac{\partial \Psi_r^{(2)}}{\partial z} - \frac{\partial \Psi_z^{(2)}}{\partial r},$$

$$U_z^{s1} = \frac{\partial \Phi^{(1)}}{\partial z} + \frac{1}{r}\frac{\partial (r\Psi_\theta^{(1)})}{\partial r} - \frac{1}{r}\frac{\partial \Psi_r^{(1)}}{\partial \theta},$$

$$U_z^{s2} = \frac{\partial \Phi^{(2)}}{\partial z} + \frac{1}{r}\frac{\partial (r\Psi_\theta^{(2)})}{\partial r} - \frac{1}{r}\frac{\partial \Psi_r^{(2)}}{\partial \theta}. \tag{33}$$

The stress components in the fluid are [19,20]

$$\sigma_{rr} = -p + (\mu_b - 2\mu/3)\Delta + 2\mu(\partial u_r/\partial r), \tag{34a}$$

$$\sigma_{r\theta} = \mu\left(\frac{1}{r}\frac{\partial u_r}{\partial \theta} + \frac{\partial u_\theta}{\partial r} - \frac{u_\theta}{r}\right), \quad \sigma_{rz} = \mu\left(\frac{\partial u_r}{\partial z} + \frac{\partial u_z}{\partial r}\right) \tag{34b}$$

and the corresponding stresses in the viscoelastic scatterer are [33]

$$\sigma_{rr}^{s1} = 2\mu_{s1}^* \frac{\partial U_r^{s1}}{\partial r} + \lambda_1^* \varepsilon_1, \quad \sigma_{rr}^{s2} = 2\mu_{s2}^* \frac{\partial U_r^{s2}}{\partial r} + \lambda_2^* \varepsilon_2,$$
$$\sigma_{r\theta}^{s1} = \mu_{s1}^* \left(\frac{1}{r} \frac{\partial U_r^{s1}}{\partial \theta} + \frac{\partial U_\theta^{s1}}{\partial r} - \frac{U_\theta^{s1}}{r} \right), \quad \sigma_{r\theta}^{s2} = \mu_{s2}^* \left(\frac{1}{r} \frac{\partial U_r^{s2}}{\partial \theta} + \frac{\partial U_\theta^{s2}}{\partial r} - \frac{U_\theta^{s2}}{r} \right),$$
$$\sigma_{rz}^{s1} = \mu_{s1}^* \left(\frac{\partial U_r^{s1}}{\partial z} + \frac{\partial U_z^{s1}}{\partial r} \right), \quad \sigma_{rz}^{s2} = \mu_{s2}^* \left(\frac{\partial U_r^{s2}}{\partial z} + \frac{\partial U_z^{s2}}{\partial r} \right), \tag{35}$$

where $\varepsilon_1 = \nabla \cdot \mathbf{U}_{s1} = \nabla^2 \Phi^{(1)} = -K_{c1}^{*2} \Phi^{(1)}$, and $\varepsilon_2 = \nabla \cdot \mathbf{U}_{s2} = \nabla^2 \Phi^{(2)} = -K_{c2}^{*2} \Phi^{(2)}$.

The appropriate boundary conditions that must hold at the interfaces are simply continuity of velocities and stresses that are written as

$$\begin{aligned}
&u_r(r,\theta,\omega)]_{r=a} = -\mathrm{i}\omega U_r^{s1}(r,\theta,\omega)]_{r=a}, \quad U_r^{s1}(r,\theta,\omega)]_{r=b} = U_r^{s2}(r,\theta,\omega)]_{r=b},\\
&u_\theta(r,\theta,\omega)]_{r=a} = -\mathrm{i}\omega U_\theta^{s1}(r,\theta,\omega)]_{r=a}, \quad U_\theta^{s1}(r,\theta,\omega)]_{r=b} = U_\theta^{s2}(r,\theta,\omega)]_{r=b},\\
&u_z(r,\theta,\omega)]_{r=a} = -\mathrm{i}\omega U_z^{s1}(r,\theta,\omega)]_{r=a}, \quad U_z^{s1}(r,\theta,\omega)]_{r=b} = U_z^{s2}(r,\theta,\omega)]_{r=b},\\
&\sigma_{rr}(r,\theta,\omega)]_{r=a} = \sigma_{rr}^{s1}(r,\theta,\omega)]_{r=a}, \quad \sigma_{rr}^{s1}(r,\theta,\omega)]_{r=b} = \sigma_{rr}^{s2}(r,\theta,\omega)]_{r=b},\\
&\sigma_{r\theta}(r,\theta,\omega)]_{r=a} = \sigma_{r\theta}^{s1}(r,\theta,\omega)]_{r=a}, \quad \sigma_{r\theta}^{s1}(r,\theta,\omega)]_{r=b} = \sigma_{r\theta}^{s2}(r,\theta,\omega)]_{r=b},\\
&\sigma_{rz}(r,\theta,\omega)]_{r=a} = \sigma_{rz}^{s1}(r,\theta,\omega)]_{r=a}, \quad \sigma_{rz}^{s1}(r,\theta,\omega)]_{r=b} = \sigma_{rz}^{s2}(r,\theta,\omega)]_{r=b}.
\end{aligned} \tag{36}$$

At this point the unknown scattering coefficients shall be determined by imposing the stated boundary conditions. Employing expansions (28)–(31) in the field equations (32)–(35), and substituting obtained results into the boundary conditions (36), one obtains, for the nth mode

$$\begin{aligned}
&-\gamma_c A_n H_n^{(1)'}(\gamma_c a) + \mathrm{i}k_z B_n H_{n+1}^{(1)}(\gamma_s a) + \frac{n}{a} C_n H_n^{(1)}(\gamma_s a),\\
&\quad + \mathrm{i}\omega \Gamma_{c1}[D_n H_n^{(1)'}(\Gamma_{c1} a) + E_n H_n^{(2)'}(\Gamma_{c1} a)] - \omega k_z [F_n H_{n+1}^{(1)}(\Gamma_{s1} a) + G_n H_{n+1}^{(2)}(\Gamma_{s1} a)]\\
&\quad + \mathrm{i}\omega \frac{n}{a} [K_n H_n^{(1)}(\Gamma_{s1} a) + L_n H_n^{(2)}(\Gamma_{s1} a)] = \phi_0 \varepsilon_n \mathrm{i}^n \gamma_c \mathrm{J}_n'(\gamma_c a),
\end{aligned} \tag{37a}$$

$$\begin{aligned}
&\frac{n}{a} A_n H_n^{(1)}(\gamma_c a) + \mathrm{i}k_z B_n H_{n+1}^{(1)}(\gamma_s a) - \gamma_s C_n H_n^{(1)'}(\gamma_s a)\\
&\quad - \mathrm{i}\omega \frac{n}{a} [D_n H_n^{(1)}(\Gamma_{c1} a) + E_n H_n^{(2)}(\Gamma_{c1} a)] - \omega k_z [F_n H_{n+1}^{(1)}(\Gamma_{s1} a) + G_n H_{n+1}^{(2)}(\Gamma_{s1} a)]\\
&\quad - \mathrm{i}\omega \Gamma_{s1} [K_n H_n^{(1)'}(\Gamma_{s1} a) + L_n H_n^{(2)'}(\Gamma_{s1} a)] = -\phi_0 \frac{n}{a} \varepsilon_n \mathrm{i}^n \mathrm{J}_n(\gamma_c a)
\end{aligned} \tag{37b}$$

$$\begin{aligned}
&-\mathrm{i}k_z a A_n H_n^{(1)}(\gamma_c a) - [(n+1) H_{n+1}^{(1)}(\gamma_s a) + \gamma_s a H_{n+1}^{(1)'}(\gamma_s a)] B_n\\
&\quad - \omega k_z a [D_n H_n^{(1)}(\Gamma_{c1} a) + E_n H_n^{(2)}(\Gamma_{c1} a)] - \mathrm{i}\omega \{[(n+1) H_{n+1}^{(1)}(\Gamma_{s1} a) + \Gamma_{s1} a H_{n+1}^{(1)'}(\Gamma_{s1} a)] F_n\\
&\quad + [(n+1) H_{n+1}^{(2)}(\Gamma_{s1} a) + \Gamma_{s1} a H_{n+1}^{(2)'}(\Gamma_{s1} a)] G_n\} = \phi_0 \varepsilon_n \mathrm{i}^{n+1} k_z a \mathrm{J}_n(\gamma_c a),
\end{aligned} \tag{37c}$$

$$[(\mathrm{i}\omega\rho - 2\mu k_c^2)H_n^{(1)''}(\gamma_c a) - 2\mu\gamma_c^2 H_n^{(1)''}(\gamma_c a)]A_n + 2\mathrm{i}\mu k_z\gamma_s H_{n+1}^{(1)'}(\gamma_s a)B_n - \frac{2\mu n}{a^2}[H_n^{(1)}(\gamma_s a) - \gamma_s a H_n^{(1)'}(\gamma_s a)]C_n - [2\mu_{s1}^*\Gamma_{c1}^2 H_n^{(1)''}(\Gamma_{c1}a) - \lambda_1^* K_{c1}^{*2} H_n^{(1)}(\Gamma_{c1}a)]D_n - [2\mu_{s1}^*\Gamma_{c1}^2 H_n^{(2)''}(\Gamma_{c1}a) - \lambda_1^* K_{c1}^{*2} H_n^{(2)}(\Gamma_{c1}a)]E_n - 2\mathrm{i}\mu_{s1}^* k_z\Gamma_{s1}[F_n H_{n+1}^{(1)'}(\Gamma_{s1}a) + G_n H_{n+1}^{(2)'}(\Gamma_{s1}a)] + \frac{2\mu_{s1}^* n}{a^2}\{[H_n^{(1)}(\Gamma_{s1}a) - \Gamma_{s1}a H_n^{(1)'}(\Gamma_{s1}a)]K_n + [H_n^{(2)}(\Gamma_{s1}a) - \Gamma_{s1}a H_n^{(2)'}(\Gamma_{s1}a)]L_n\} = -\phi_0\varepsilon_n\mathrm{i}^n[(\mathrm{i}\omega\rho - 2\mu k_c^2)\mathrm{J}_n(\gamma_c a) - 2\mu\gamma_c^2\mathrm{J}_n''(\gamma_c a)], \tag{37d}$$

$$-2\mu n[H_n^{(1)}(\gamma_c a) - a\gamma_c H_n^{(1)'}(\gamma_c a)]A_n - \mathrm{i}k_z\mu[(n+1)aH_{n+1}^{(1)}(\gamma_s a) - \gamma_s a^2 H_{n+1}^{(1)'}(\gamma_s a)]B_n - \mu[n^2 H_n^{(1)}(\gamma_s a) + \gamma_s^2 a^2 H_n^{(1)''}(\gamma_s a) - a\gamma_s H_n^{(1)'}(\gamma_s a)]C_n - 2\mu_{s1}^* n\{[H_n^{(1)}(\Gamma_{c1}a) - a\Gamma_{c1}H_n^{(1)'}(\Gamma_{c1}a)]D_n + [H_n^{(2)}(\Gamma_{c1}a) - a\Gamma_{c1}H_n^{(2)'}(\Gamma_{c1}a)]E_n\} + \mathrm{i}k_z\mu_{s1}^*\{[(n+1)aH_{n+1}^{(1)}(\Gamma_{s1}a) - \Gamma_{s1}a^2 H_{n+1}^{(1)'}(\Gamma_{s1}a)]F_n + [(n+1)aH_{n+1}^{(2)}(\Gamma_{s1}a) - \Gamma_{s1}a^2 H_{n+1}^{(2)'}(\Gamma_{s1}a)]G_n\} + \mu_{s1}^*[n^2 H_n^{(1)}(\Gamma_{s1}a) + \Gamma_{s1}^2 a^2 H_n^{(1)''}(\Gamma_{s1}a) - a\Gamma_{s1}H_n^{(1)'}(\Gamma_{s1}a)]K_n + \mu_{s1}^*[n^2 H_n^{(2)}(\Gamma_{s1}a) + \Gamma_{s1}^2 a^2 H_n^{(2)''}(\Gamma_{s1}a) - a\Gamma_{s1}H_n^{(2)'}(\Gamma_{s1}a)]L_n = 2\mu n\phi_0\varepsilon_n\mathrm{i}^n[\mathrm{J}_n(\gamma_c a) - a\gamma_c\mathrm{J}_n'(\gamma_c a)], \tag{37e}$$

$$-2\mathrm{i}k_z\mu a^2\gamma_c A_n H_n^{(1)'}(\gamma_c a) + \mu\{[n+1-a^2k_z^2]H_{n+1}^{(1)}(\gamma_s a) - \gamma_s a(n+1)H_{n+1}^{(1)'}(\gamma_s a) - \gamma_s^2 a^2 H_{n+1}^{(1)''}(\gamma_s a)\}B_n + \mathrm{i}k_z\mu anC_n H_n^{(1)}(\gamma_s a) - 2\mathrm{i}k_z\mu_{s1}^* a^2\Gamma_{c1}[D_n H_n^{(1)'}(\Gamma_{c1}a) + E_n H_n^{(2)'}(\Gamma_{c1}a)] - \mu_{s1}^*\{[n+1-a^2k_z^2]H_{n+1}^{(1)}(\Gamma_{s1}a) - \Gamma_{s1}a(n+1)H_{n+1}^{(1)'}(\Gamma_{s1}a) - \Gamma_{s1}^2 a^2 H_{n+1}^{(1)''}(\Gamma_{s1}a)\}F_n - \mu_{s1}^*\{[n+1-a^2k_z^2]H_{n+1}^{(2)}(\Gamma_{s1}a) - \Gamma_{s1}a(n+1)H_{n+1}^{(2)'}(\Gamma_{s1}a) - \Gamma_{s1}^2 a^2 H_{n+1}^{(2)''}(\Gamma_{s1}a)\}G_n - \mathrm{i}k_z\mu_{s1}^* an[K_n H_n^{(1)}(\Gamma_{s1}a) + L_n H_n^{(2)}(\Gamma_{s1}a)] = 2\phi_0\mu a^2\varepsilon_n\mathrm{i}^{n+1}k_z\gamma_c\mathrm{J}_n'(\gamma_c a), \tag{37f}$$

$$\Gamma_{c1}[D_n H_n^{(1)'}(\Gamma_{c1}b) + E_n H_n^{(2)'}(\Gamma_{c1}b)] + \mathrm{i}k_z[F_n H_{n+1}^{(1)}(\Gamma_{s1}b) + G_n H_{n+1}^{(2)}(\Gamma_{s1}b)] + \frac{n}{b}[K_n H_n^{(1)}(\Gamma_{s1}b) + L_n H_n^{(2)}(\Gamma_{s1}b)] - \Gamma_{c2}M_n\mathrm{J}_n'(\Gamma_{c2}b) - \mathrm{i}k_z N_n\mathrm{J}_{n+1}(\Gamma_{s2}b) - \frac{n}{b}Q_n\mathrm{J}_n(\Gamma_{s2}b) = 0, \tag{37g}$$

$$-\frac{n}{b}[D_n H_n^{(1)}(\Gamma_{c1}b) + E_n H_n^{(2)}(\Gamma_{c1}b)] + \mathrm{i}k_z[F_n H_{n+1}^{(1)}(\Gamma_{s1}b) + G_n H_{n+1}^{(2)}(\Gamma_{s1}b)] - \Gamma_{s1}[K_n H_n^{(1)'}(\Gamma_{s1}b) + L_n H_n^{(2)'}(\Gamma_{s1}b)] + \frac{n}{b}M_n\mathrm{J}_n(\Gamma_{c2}b) - \mathrm{i}k_z N_n\mathrm{J}_{n+1}(\Gamma_{s2}b) + \Gamma_{s2}Q_n\mathrm{J}_n'(\Gamma_{s2}b) = 0, \tag{37h}$$

$$\mathrm{i}k_z b[D_n H_n^{(1)}(\Gamma_{c1}b) + E_n H_n^{(2)}(\Gamma_{c1}b)] - [(n+1)H_{n+1}^{(1)}(\Gamma_{s1}b) + \Gamma_{s1}bH_{n+1}^{(1)'}(\Gamma_{s1}b)]F_n - [(n+1)H_{n+1}^{(2)}(\Gamma_{s1}b) + \Gamma_{s1}bH_{n+1}^{(2)'}(\Gamma_{s1}b)]G_n - \mathrm{i}k_z bM_n\mathrm{J}_n(\Gamma_{c2}b) + [(n+1)\mathrm{J}_{n+1}(\Gamma_{s2}b) + \Gamma_{s2}b\mathrm{J}_{n+1}'(\Gamma_{s2}b)]N_n = 0, \tag{37i}$$

$$[-\lambda_1^* K_{c1}^{*2} H_n^{(1)}(\Gamma_{c1}b) + 2\mu_{s1}^* \Gamma_{c1}^2 H_n^{(1)''}(\Gamma_{c1}b)]D_n + [-\lambda_1^* K_{c1}^{*2} H_n^{(2)}(\Gamma_{c1}b) + 2\mu_{s1}^* \Gamma_{c1}^2 H_n^{(2)''}(\Gamma_{c1}b)]E_n$$
$$+ 2ik_z \mu_{s1}^* \Gamma_{s1}[F_n H_{n+1}^{(1)'}(\Gamma_{s1}b) + G_n H_{n+1}^{(2)'}(\Gamma_{s1}b)] - \frac{2\mu_{s1}^* n}{b^2}\{[H_n^{(1)}(\Gamma_{s1}b) - b\Gamma_{s1} H_n^{(1)'}(\Gamma_{s1}b)]K_n$$
$$+ [H_n^{(2)}(\Gamma_{s1}b) - b\Gamma_{s1} H_n^{(2)'}(\Gamma_{s1}b)]L_n\} - [-\lambda_2^* K_{c2}^{*2} \mathrm{J}_n(\Gamma_{c2}b) + 2\mu_{s2}^* \Gamma_{c2}^2 \mathrm{J}_n''(\Gamma_{c2}b)]M_n$$
$$- 2ik_z \mu_{s2}^* \Gamma_{s2} N_n \mathrm{J}_{n+1}'(\Gamma_{s2}b) + \frac{2\mu_{s2}^* n}{b^2}[\mathrm{J}_n(\Gamma_{s2}b) - b\Gamma_{s2}\mathrm{J}_n'(\Gamma_{s2}b)]Q_n = 0, \tag{37j}$$

$$2\mu_{s1}^* n\{[H_n^{(1)}(\Gamma_{c1}b) - b\Gamma_{c1} H_n^{(1)'}(\Gamma_{c1}b)]D_n + [H_n^{(2)}(\Gamma_{c1}b) - b\Gamma_{c1} H_n^{(2)'}(\Gamma_{c1}b)]E_n\}$$
$$- ik_z \mu_{s1}^* \{[(n+1)bH_{n+1}^{(1)}(\Gamma_{s1}b) - \Gamma_{s1} b^2 H_{n+1}^{(1)'}(\Gamma_{s1}b)]F_n + [(n+1)bH_{n+1}^{(2)}(\Gamma_{s1}b)$$
$$- \Gamma_{s1} b^2 H_{n+1}^{(2)'}(\Gamma_{s1}b)]G_n\} - \mu_{s1}^*[n^2 H_n^{(1)}(\Gamma_{s1}b) + \Gamma_{s1}^2 b^2 H_n^{(1)''}(\Gamma_{s1}b)$$
$$- b\Gamma_{s1} H_n^{(1)'}(\Gamma_{s1}b)]K_n - \mu_{s1}^*[n^2 H_n^{(2)}(\Gamma_{s1}b) + \Gamma_{s1}^2 b^2 H_n^{(2)''}(\Gamma_{s1}b) - b\Gamma_{s1} H_n^{(2)'}(\Gamma_{s1}b)]L_n$$
$$- 2\mu_{s2}^* n[\mathrm{J}_n(\Gamma_{c2}b) - b\Gamma_{c2}\mathrm{J}_n'(\Gamma_{c2}b)]M_n + ik_z \mu_{s2}^*[(n+1)b\mathrm{J}_{n+1}(\Gamma_{s2}b)$$
$$- \Gamma_{s2} b^2 \mathrm{J}_{n+1}'(\Gamma_{s2}b)]N_n + \mu_{s2}^*[n^2 \mathrm{J}_n(\Gamma_{s2}b) + \Gamma_{s2}^2 b^2 \mathrm{J}_n''(\Gamma_{s2}b) - b\Gamma_{s2}\mathrm{J}_n'(\Gamma_{s2}b)]Q_n = 0, \tag{37k}$$

$$2ik_z \mu_{s1}^* b^2 \Gamma_{c1}[D_n H_n^{(1)'}(\Gamma_{c1}b) + E_n H_n^{(2)'}(\Gamma_{c1}b)] + \mu_{s1}^*\{[n+1-b^2k_z^2]H_{n+1}^{(1)}(\Gamma_{s1}b)$$
$$- \Gamma_{s1} b(n+1)H_{n+1}^{(1)'}(\Gamma_{s1}b) - \Gamma_{s1}^2 b^2 H_{n+1}^{(1)''}(\Gamma_{s1}b)\}F_n + \mu_{s1}^*\{[n+1-b^2k_z^2]H_{n+1}^{(2)}(\Gamma_{s1}b)$$
$$- \Gamma_{s1} b(n+1)H_{n+1}^{(2)'}(\Gamma_{s1}b) - \Gamma_{s1}^2 b^2 H_{n+1}^{(2)''}(\Gamma_{s1}b)\}G_n + ik_z \mu_{s1}^* bn[K_n H_n^{(1)}(\Gamma_{s1}b) + L_n H_n^{(2)}(\Gamma_{s1}b)]$$
$$- 2ik_z \mu_{s2}^* b^2 \Gamma_{c2} M_n \mathrm{J}_n'(\Gamma_{c2}b) - \mu_{s2}^*\{[n+1-b^2k_z^2]\mathrm{J}_{n+1}(\Gamma_{s2}b) - \Gamma_{s2} b(n+1)\mathrm{J}_{n+1}'(\Gamma_{s2}b)$$
$$- \Gamma_{s2}^2 b^2 \mathrm{J}_{n+1}''(\Gamma_{s2}b)\}N_n - ik_z \mu_{s2}^* bnQ_n \mathrm{J}_n(\Gamma_{s2}b) = 0 \tag{37l}$$

where $n = 0, 1, 2, \ldots$, except for Eqs. (37b, e, h, k) where $n = 1, 2, \ldots$.

6. Numerical results

In order to illustrate the nature and general behaviour of the solution, a numerical example is considered in this section. Realizing the large number of parameters involved here, no attempt is made to exhaustively evaluate the effect of varying each of them. The intention is merely to illustrate the kinds of results to be expected from some representative and physically realistic choices of values for these parameters. From these data some trends are noted and general conclusions made about the relative importance of certain parameters. Noting the crowd of parameters that enter into the final expressions and keeping in view the availability of numerical data, attention will be confined to a particular model. The surrounding fluid is taken to be glycerine with its assumed properties displayed in Table 1 [36]. As there are no reliable data found for the bulk viscosity of glycerine, its numerical value is presumed to be nearly equal to that of the shear viscosity. The scatterer core material is taken to be stainless steel and the viscoelastic coating is assumed to be elastomeric with a fixed outer radius of $a = 0.05$ cm. Hartmann et al. [30], reported for the first time, all the input parameters necessary for a complete description of viscoelastic material properties for a set of (polyurethane) polymers within the context of Havriliak–Negami (HN) theory. The HN fitting parameters for two selected polymers with

Table 1
Parameter values used in calculations

Parameter	Glycerine	Water
μ (kg/m.s)	0.95	0.000894
μ_b (kg/m.s)	0.95	0.00250
c (m/s)	1.91×10^3	1.48×10^3
ρ (kg/m^3)	1250	1000

Table 2
Havriliak–Negami fitting parameters [30]

Parameter	Polymer 18	Polymer 19
G_0 (Pa)	3.372×10^6	5.019×10^6
G_∞ (Pa)	1.453×10^9	0.8089×10^9
ρ_s (kg/m^3)	1101	1096
τ (s)	3.139×10^{-9}	1.702×10^{-1}
α	0.4822	0.4941
β	0.4116	0.1356
ν	0.4	0.4

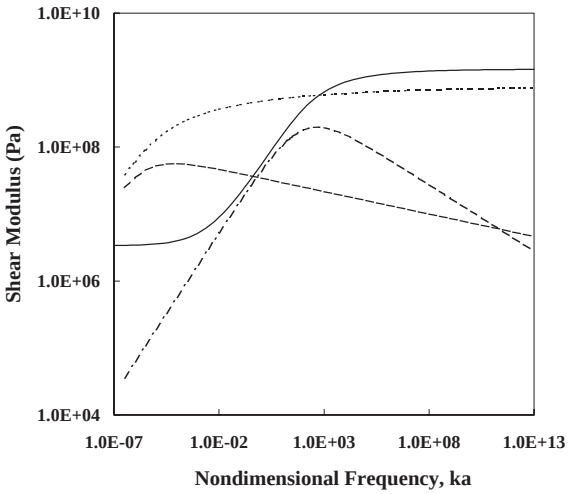

Fig. 2. The HN-fit for real and imaginary parts of the shear modulus for the selected polymers in a wide frequency range [— $G'(\omega)$, Polymer 18; _.-._ $G''(\omega)$, Polymer 18; _ _ _ $G'(\omega)$, Polymer 19; …… $G''(\omega)$, Polymer 19].

distinctively different dynamic viscoelastic properties in the frequency range of interest are compiled in Table 2. The corresponding fit of HN equations for real and imaginary parts of the shear modulus (e.g., Eqs. (1)), for the selected polymers in a wide frequency range, are displayed in Fig. 2. It is clear that polymer 18 has a relatively high damping (i.e., loss factor or $\eta(\omega) = G''(\omega)/G'(\omega)$), as compared with polymer 19, in the frequency range of interest

$(0.1 < ka < 10)$. Accurate computation of Bessel functions of complex argument is achieved using MATLAB specialized math functions "besselh" and "besselj". The derivatives of Bessel functions were calculated by utilizing (9.1.27), (10.1.19) and (10.1.22) in Ref. [35]. Two separate MATLAB codes were constructed to calculate the unknown scattering coefficients and relevant acoustic field quantities as functions of non-dimensional frequency $ka = \omega a/c$ for the coated sphere and the coated cylinder, respectively.

The most relevant acoustic field quantities are the scattered farfield pressure and the scattering form-function. Using Eq. (24), the scattered farfield pressure amplitude is simply written as

$$|p_{\infty}^{scat}(r,\theta,\omega)| = \lim_{r\to\infty} |-\mathrm{i}\omega\rho\varphi_c(r,\theta,\omega) + k_c^2(\mu_b + \tfrac{4}{3}\mu)\varphi_c(r,\theta,\omega)|. \tag{38}$$

The standard definition of the (farfield) form-function amplitude is given by [5]

$$|f_{\infty}(r,\theta,\omega)| \equiv \lim_{r\to\infty} \left| \left(\frac{2r}{a}\right)^{1/\zeta} \frac{\varphi_c(r,\theta,\omega)}{\phi_0} \right|, \tag{39}$$

where $\zeta = 1$ ($\zeta = 2$) for acoustic scattering from the compound sphere (cylinder). Fig. 3 displays the angular distribution of the scattered farfield pressure (i.e., $|p_{\infty}^{scat}(r,\theta,\omega)|/\rho c^2$) for a unit amplitude plane wave ($\phi_0 = 1.$) incident upon a compound sphere with a steel core and an elastomeric coating immersed in glycerine at selected dimensionless wave numbers and coating

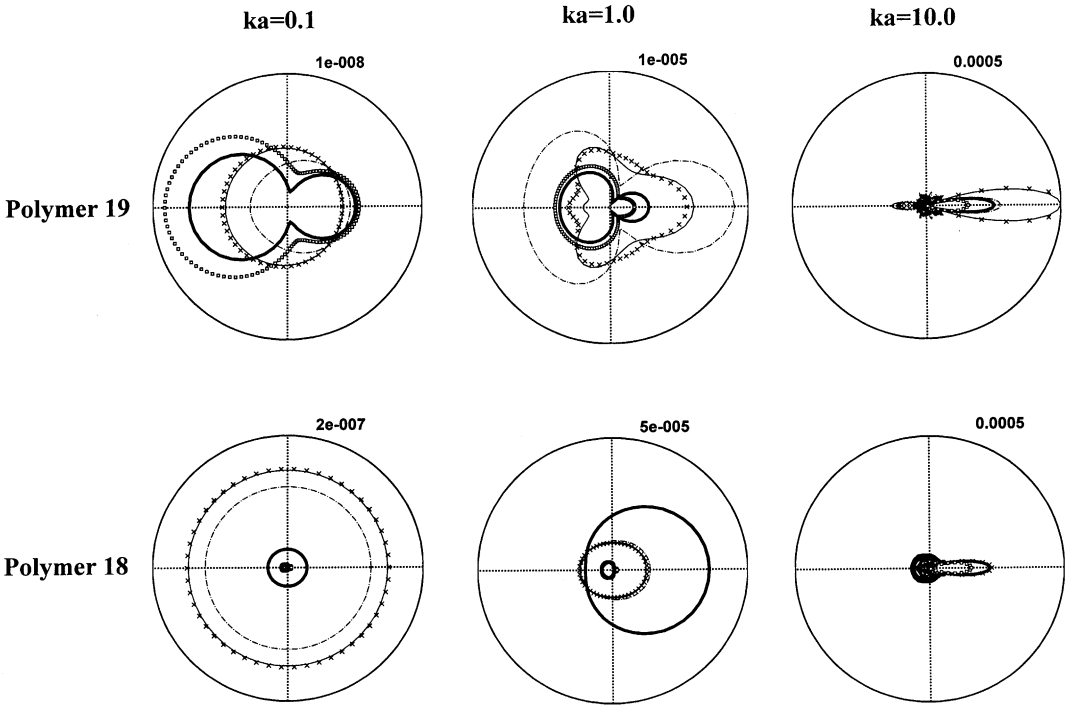

Fig. 3. Normalized farfield scattered pressure directivity patterns, $|p_{scat.}(r_{\infty},\theta)|/\rho c^2$, for a viscoelastically coated steel sphere immersed in glycerine at selected dimensionless wave numbers and coating thicknesses [□ $b/a = 1$ (solid steel); —— $b/a = 0.9$; _.-._ $b/a = 0.5$; — $b/a = 0.2$; × $b/a = 0$ (solid polymer)] .

thicknesses. The farfield value of the radial co-ordinate in each case was simply chosen by making several computer runs while seeking for the convergence of the scattered pressure directivity patterns. The choice of $r_\infty = 10a$ was found to be adequate for all cases. Furthermore, a maximum number of 40 modes were included in all summations in order to assure convergence in the high frequencies. It is very interesting to notice the change in directionality of the scattered waves as the frequency is varied. As seen from the figure, at low and intermediate frequencies (i.e., at $ka = 0.1, 1$) increasing the thickness of the polymeric coating 19 causes a noticeable decrease in the scattered farfield pressure directionality. At these frequencies, the polymeric coating 18, which has the highest loss factor in our frequency range of interest, leads to almost uniform directivity patterns for all coating thicknesses. As the frequency increases to $ka = 10$, the pressure patterns become highly directional, especially for the polymeric coating 19 that has a relatively low damping. At this frequency, the scattered farfield pressure associated with the polymeric coating 18 is comparatively less directional and it seems to be nearly independent of the coating thickness. The most surprizing observation is perhaps the fact that the scattered pressure magnitudes for the coated sphere 18 (sphere 19) are on the whole distinctly higher than (comparable to) that of the solid steel sphere, especially at low and intermediate frequencies. A physical explanation for this apparently non-trivial result is presented below.

Fig. 4 displays the variation of the backward-scattered farfield pressure magnitude (i.e., $|f_\infty(r, \theta, \omega)|_{\theta=\pi}$, or the form function amplitude) with nondimensional frequency and coating thickness. Here it is noted that $b/a = 1$ refers to a solid steel sphere with no coating and $b/a = 0$ is a simple elastomeric sphere. The main observation for polymeric coating 18 is the presence of a single relatively wide peak for each coating thickness at lower frequencies (i.e., $ka < 1.7$). As the coating thickness increases (b/a decreases), the peaks in the form function curves drop considerably as they to shift to lower frequencies. For $b/a < 0.6$ there are almost no resonances in the intermediate frequencies and only a relatively small peak is observed near $ka \approx 0.4$. In case of the polymeric coating 19, on the other hand, the resonance frequencies significantly depend on the coating thickness and there are numerous relatively sharp resonances observed in the low to intermediate frequencies. The observed oscillatory behaviour is due to the effect of acoustic resonant scattering, i.e., when an acoustic wave is incident upon an object, the wave induces the eigenmode oscillation of the object and the motion of the object, in turn, affects the scattering pattern of the wave [37]. As the thickness of the polymeric coating 19 decreases, these resonances begin to become wider (fewer) as they shift to lower frequencies, and eventually in case of the solid steel sphere there are no perceptible resonance peaks observed in the frequency range of our interest. The above observations suggest that the characteristically high (moderate) scattered pressure magnitudes observed in Fig. 3 for the polymeric sphere 18 (sphere 19) at low and intermediate frequencies, in comparison with the solid steel sphere case, is a direct consequence of acoustic resonant scattering effects at these frequencies.

The seemingly unusual results obtained in Fig. 3 may further be clarified if the eigenfrequencies of a solid sphere is studied. Ye [38] considered the problem of free vibration of a solid elastic sphere and deduced the corresponding exact eigenfrequency equation (see their Eqs. (16)) using the standard textbook (infinite series) approach. Extension of the latter work to determine the general eigenfrequency equation of a viscoelastic sphere is quite straightforward. Therefore, following Ye's approach in solving the corresponding boundary value problem, the eigenfrequency equation associated with general free oscillations of a solid viscoelastic sphere

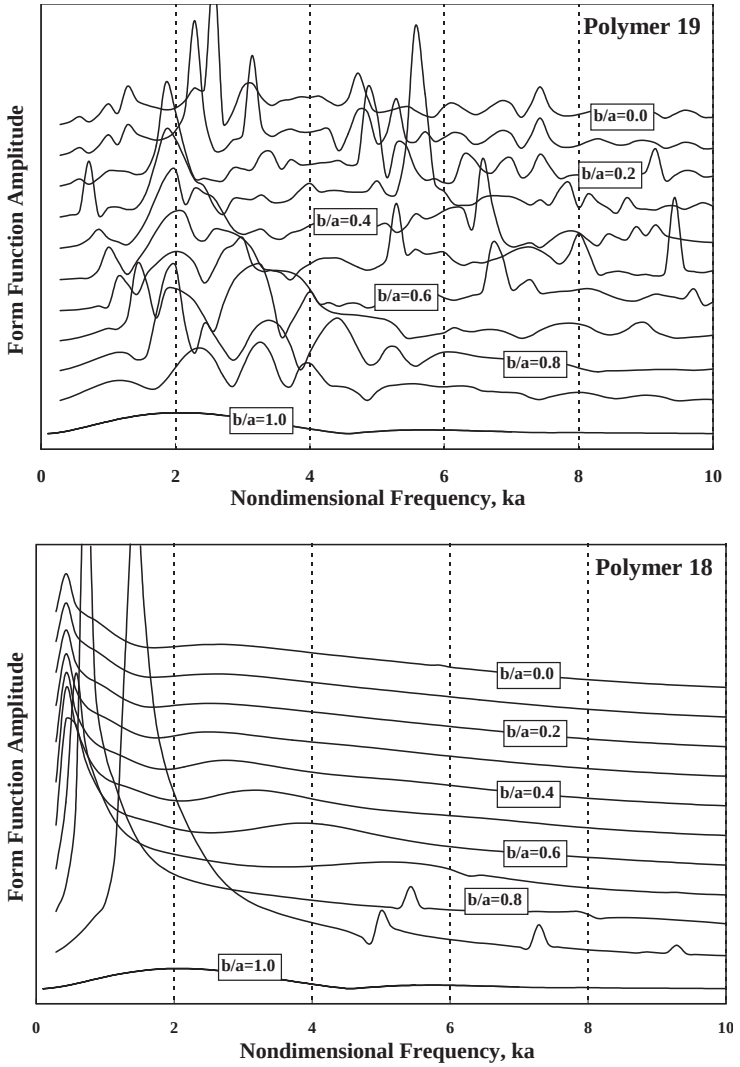

Fig. 4. The variation of the form function amplitude with non-dimensional frequency and coating thickness for a compound sphere.

(after some manipulations) is obtained as

$$\det\begin{vmatrix} K_c^{*2}[2\mu_s^*(\omega)\mathrm{j}_n''(K_c^*a)-\lambda^*(\omega)\mathrm{j}_n(K_c^*a)] & \dfrac{2n(n+1)\mu_s^*(\omega)}{a^2}[aK_s^*\mathrm{j}_n'(K_s^*a)-\mathrm{j}_n(K_s^*a)] \\ \dfrac{2}{a^2}\mathrm{j}_n(K_c^*a)-\dfrac{2}{a}K_c^*\mathrm{j}_n'(K_c^*a) & \dfrac{2-n(n+1)}{a^2}\mathrm{j}_n(K_s^*a)-K_s^{*2}\mathrm{j}_n''(K_s^*a)] \end{vmatrix}=0. \quad (40)$$

Eigenequation (40) is solvable numerically. However, due to the oscillatory behaviour of the Bessel functions, there are an infinite number of eigenfrequencies associated with each multipole n. Table 3 compares the first four (non-zero) eigenfrequencies associated with the $n=0$ (monopole or spheroidal) and $n=1$ (dipole or toroidal) modes of polymeric sphere's oscillation with that of

Table 3
Comparison between the computed eigenfrequencies of the polymeric spheres with those of steel sphere

Mode number	Polymer 18	Polymer 19	Stainless steel
$n = 0$	$0.346 + 0.964i$	$0.852 + 0.0316i$	4.203
	$0.663 + 0.307i$	$2.106 + 0.0705i$	8.540
	$1.163 + 0.532i$	$3.285 + 0.105i$	10.187
	$1.653 + 0.607i$	$4.450 + 0.137i$	15.746
$n = 1$	$0.361 + 0.167i$	$1.300 + 0.0459i$	6.034
	$0.873 + 0.402i$	$2.616 + 0.0855i$	12.139
	$1.453 + 0.660i$	$3.915 + 0.122i$	13.808
	$1.983 + 0.889i$	$5.005 + 0.152i$	18.316

the solid stainless steel sphere. These results are generated using a MATLAB code that was developed on the basis of an automatic root-searching algorithm in the complex plane. Examination of the numerical data in Table 3 further confirms that the typically high (moderate) scattered pressure amplitudes for the polymeric sphere 18 (sphere 19) in comparison with the solid steel sphere case, especially at low and intermediate frequencies, is due to the fact that the eigenfrequencies associated with the (visco)elastic resonances of the solid steel sphere (coated spheres) predominantly fall outside (inside) this frequency range. Furthermore, comparatively high imaginary parts for the computed eigenfrequencies of the polymeric sphere 18 (i.e., high damping in the associated eigenmodes [39]) are noticed, which explains the relatively wide resonances observed in the corresponding form function plot. In addition, repeating the above analysis for a submerged solid sphere is numerically checked to yield roughly the same eigenfrequencies, especially for the $n = 0$ (monopole) mode.

In order to check the overall validity of the first part of the work it was initially noted that the farfield scattered pressure directivity patterns associated with the solid polymers as noted by cross-markers ($b/a = 0$) in Fig. 3, accurately duplicate the numerical results shown in Figs. 3, 4 and 6 in Ref. [22]. Furthermore, keeping in mind the lack of any reliable numerical results for acoustic scattering from a compound elastic sphere in the literature, a general MATLAB code was used to compute the angular distribution of the form function amplitude ($|f_\infty(r, \theta, \omega)|$) for a compound sphere with a polystyrene core and an elastomeric coating of the same material immersed in water (Table 1) at selected dimensionless wave numbers ($ka = 1, 10$). The numerical results, as displayed in Fig. 5, reasonably well follow the (approximate) T-matrix results for scattering from a solid polystyrene sphere immersed in (inviscid) water (see Fig. 54, p. 265 in Ref. [5]).

Fig. 6 displays the angular distribution of the scattered farfield pressure due to normal incidence ($\alpha = 0$) of a unit amplitude ($\phi_0 = 1.$) plane wave on a compound cylinder with a steel core and elastomeric coating immersed in glycerine at selected dimensionless wave numbers and coating thicknesses. Here, observations analogous to the coated sphere case (Fig. 3) can be made. In particular, the patterns are very uniform at the lowest frequency, especially for the coated cylinder 18. At this frequency, increasing the thickness of the polymeric coating 19 causes a noticeable decrease in the scattered farfield pressure directionality, while the polymeric coating 18, which has the highest loss factor in the frequency range of interest, leads to almost circular directivity patterns for all coating thicknesses. As the frequency increases, the patterns become

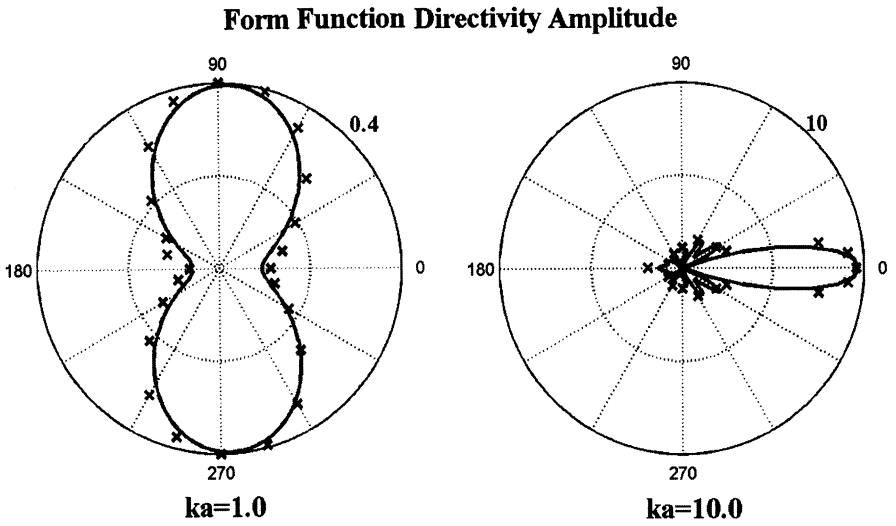

Fig. 5. The angular distribution of the form function amplitude for a solid polystyrene sphere immersed in water at selected dimensionless wave numbers (—— MATLAB Code; × T-matrix results [5]).

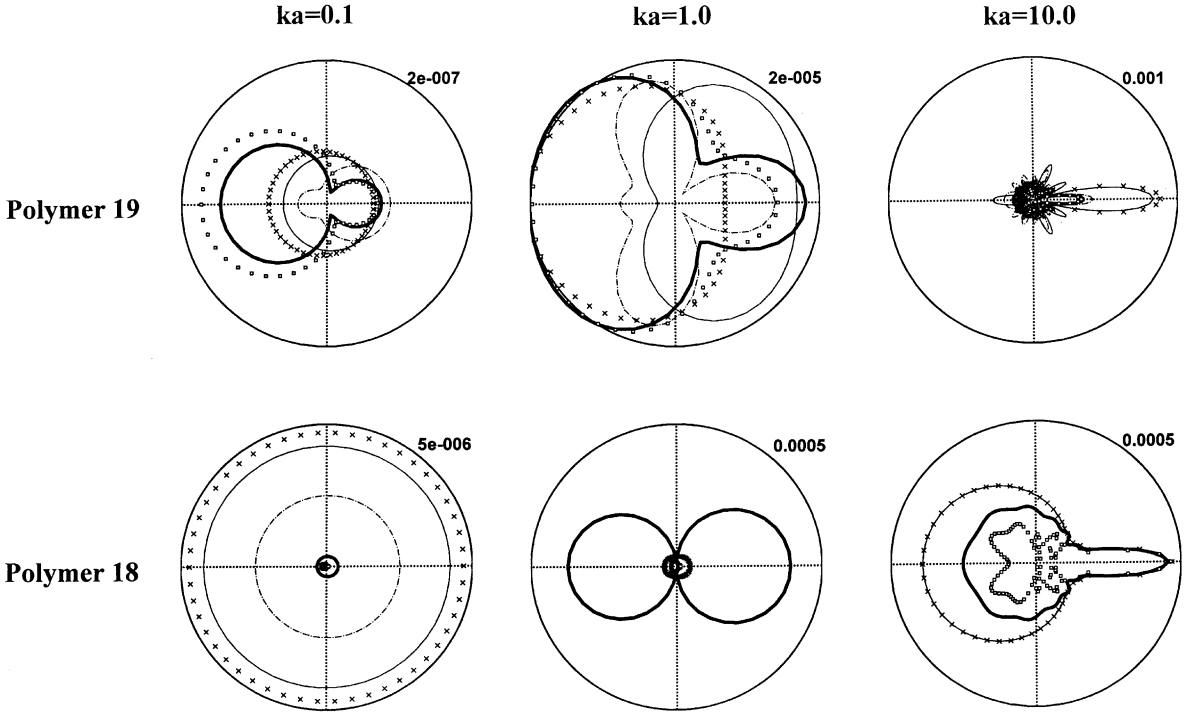

Fig. 6. Normalized farfield scattered pressure directivity patterns, $|p_{scat.}(r_\infty,\theta)|/\rho c^2$, for a viscoelastically coated steel cylinder immersed in glycerine at selected dimensionless wave numbers and coating thicknesses [□ $b/a = 1$ (solid steel); —— $b/a = 0.9$; _·_·_ $b/a = 0.5$; — $b/a = 0.2$; × $b/a = 0$ (solid polymer)].

more directional while their magnitudes considerably increase, especially for the polymeric coating 19 that has a relatively low damping. In addition, relatively high back-scattered pressure amplitudes for both polymeric cylinders at the intermediate and large frequencies (i.e., at $ka = 1, 10$) are noted. The most notable observation is, once more, the distinctly high scattered pressure magnitudes for the coated cylinder 18 in comparison with the solid steel cylinder, especially at low and intermediate frequencies. The physical explanation of this effect can be discussed as in the case of the polymeric sphere.

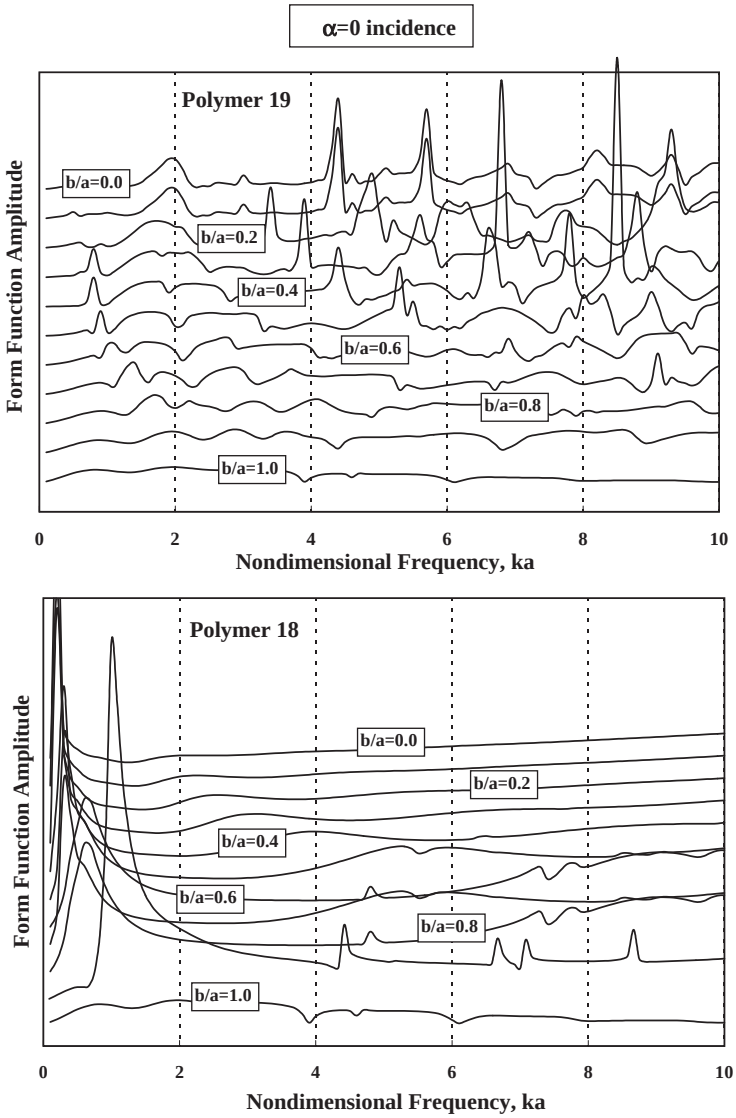

Fig. 7. The variations of the form function amplitude with non-dimensional frequency and coating thickness for normal wave incidence ($\alpha = 0$) incident upon the coated cylinder.

Fig. 7 displays the variations of the form function amplitude with non-dimensional frequency and coating thickness for normal wave incidence ($\alpha = 0$) upon the coated cylinder. Similar to the coated sphere case, the main observation for coated cylinder 18 is that the resonances in the form function curves begin to shift to very low frequencies as the coating thickness increases. For this polymer for $b/a < 0.2$, there are no significant resonances at the intermediate and high frequencies while a single fundamental peak is observed near $ka \approx 0.2$. Furthermore, the form function curves for $b/a \leqslant 0.8$ gradually rise as the frequency increases. The latter observation is in agreement with the relatively large back-scattering pressure amplitude noted for coated cylinder 18 at $ka = 10$ in Fig. 6. For the coated cylinder 19, on the other hand, very few relatively small magnitude resonances are observed for small coating thicknesses (i.e., $b/a > 0.6$). As the coating thickness is increased, the magnitude and number of these resonances increase especially in the intermediate and high-frequency range. Fig. 8 displays the 6form function amplitude curves for oblique ($\alpha = \pi/4$) wave incidence upon the coated cylinder. Remarks similar to above discussion can be made. It is clear that the resonance frequencies of the coated cylinder 18 (cylinder 19) are somewhat (moderately) dependent on the angle of incidence. In particular, the main effect of increasing the angle of incidence on the form function curves of the coated cylinder 18 (cylinder 19) seems to be the slight (modest) shift in the resonant peaks to the lower frequencies.

Finally, to check overall validity of the second part of the work a general MATLAB code was used for the coated cylinder to compute the form function amplitude (i.e., $\sqrt{2r_\infty/a}\,|p_\infty^{scat}(r,\theta,\omega)/(-i\omega\rho)\phi_0|_{\theta=\pi}\exp(-ikr_\infty\cos\alpha)$, as defined in Ref. [40]), versus non-dimensional frequency for oblique plane wave incidence ($\alpha = 0, \pi/6$) upon a copper-clad aluminium rod immersed in water. Physical properties of the cladding and the core materials are assumed as in Table 1 in Ref. [40]. The outer radius of the clad rod is $a = 0.915$ cm and its core radius is $b = 0.870$ cm. Fig. 9 demonstrates that the numerical results closely follow the numerical data extracted from Fig. 2 in Ref. [40].

7. Conclusions

This work presents analytical solutions as well as numerical results for the boundary value problem concerning the interaction of a plane sound wave with a coated sphere and a coated cylinder immersed in viscous fluids. The prime objective is to investigate the effects of dynamic viscoelastic properties of coating material on acoustic scattering and its associated quantities. Numerical results reveal that for the (low-damping) polymeric coating 19, the scattered farfield pressure directivity patterns at small and intermediate non-dimensional frequencies are highly dependent on the coating thickness. At these frequencies, the polymeric coating 18, which has the highest loss factor in the frequency range of interest, leads to very uniform pressure patterns for essentially all coating thicknesses. Furthermore, the scattered pressure magnitudes associated with this polymer are on the whole distinctly higher than that of the solid steel scatterer, especially at the lowest frequency. The physical rationalization for this apparently non-trivial result is associated with acoustic resonant scattering effects by noting the presence of a fundamental peak in the corresponding form function amplitude plots at relatively low frequencies. The situation is clarified more by studying free vibration of a solid (visco)elastic sphere. Numerical solution of the resultant eigenfrequency equation further confirms that the comparatively high (moderate)

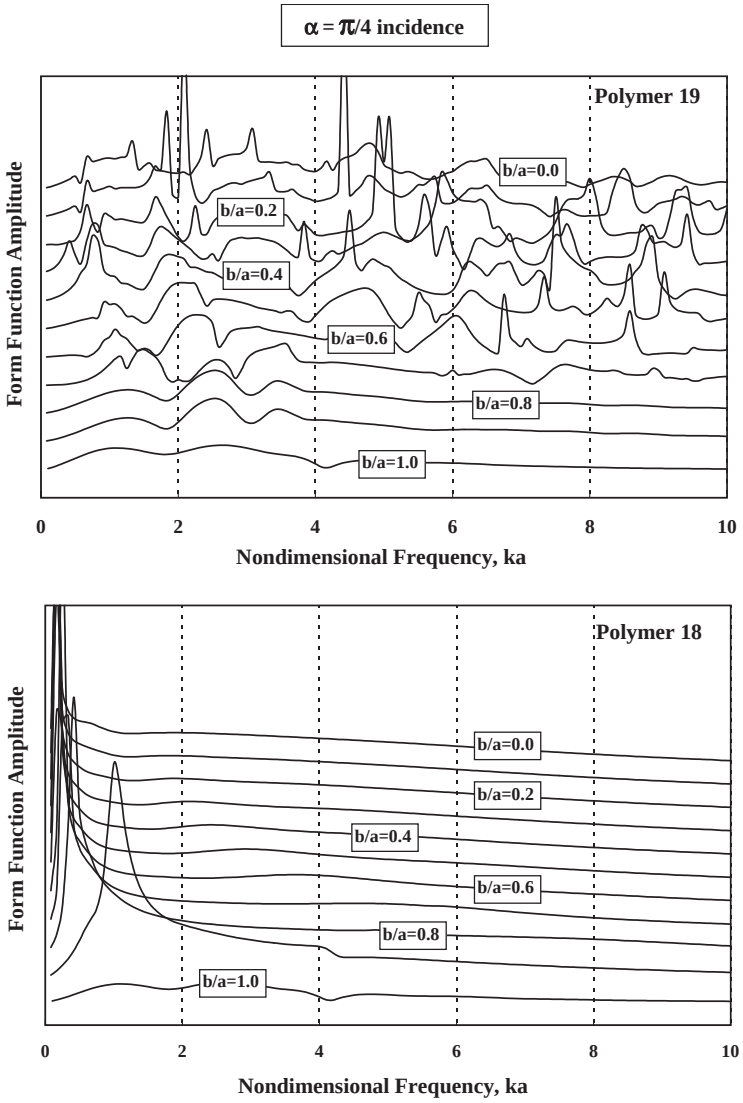

Fig. 8. The variations of the form function amplitude with non-dimensional frequency and coating thickness for $\alpha = \pi/4$ upon the coated cylinder.

scattered farfield pressure amplitudes observed for the polymeric sphere 18 (sphere 19) at low and intermediate frequencies is because the eigenfrequencies associated with (visco)elastic resonances of the coated spheres (solid steel sphere) predominantly fall inside (outside) this frequency range. The proposed model can lead to a better understanding of dynamic response of compound viscoelastic scatterers in an acoustic field. It may be equally useful in complementing the nondestructive evaluation (NDE) [25] and inverse scattering [41] techniques that have been developed to characterize the physical properties of viscoelastic materials (coatings) from laboratory measurements of scattered acoustic field.

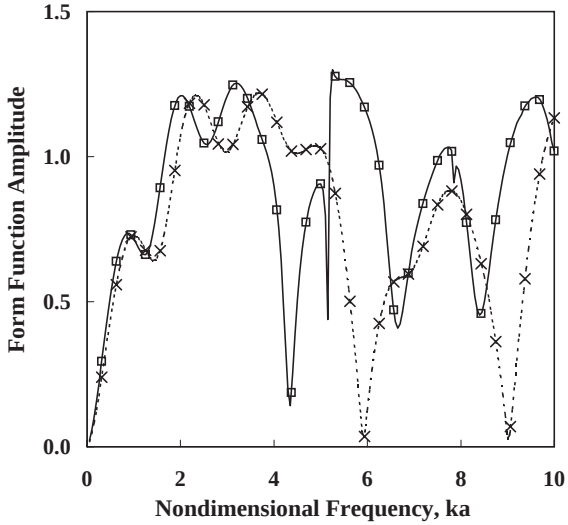

Fig. 9. Calculated form function versus non-dimensional frequency for oblique wave incidence upon a copper-clad aluminium rod in water (— MATLAB Code, $\alpha = 0$; ····· MATLAB Code, $\alpha = \pi/6$; □ Honarvar and Sinclair's results, $\alpha = 0$; × Honarvar and Sinclair's results, $\alpha = \pi/6$ [40]).

Acknowledgements

The authors wish to sincerely thank professors Daniel Levesque, Roderic Lakes, Yves Berthelot, S. Temkin, and Andrei Dukhin for valuable and productive consultations on dynamic theory of viscoelasticity and acoustics of (thermo)viscous media. They are also indebted to the demanding reviewers whose constructive critiques lead to substantial improvement of the manuscript.

References

[1] Lord Rayleigh, *Theory of Sound* (two volumes), Dover Publications, New York, 1945.
[2] Sir H. Lamb, *Hydrodynamics*, Dover Publications, New York, 1945.
[3] P.M. Morse, *Vibration and Sound*, McGraw-Hill, New York, 1948.
[4] J.J. Faran, Sound scattering by solid cylinders and spheres, *Journal of the Acoustical Society of America* 23 (1951) 405–418.
[5] V.V. Varadan, Y. Ma, V.K. Varadan, A. Lakhtakia, Scattering of waves by spheres and cylinders, in: V.V. Varadan, A. Lakhtakia, V.K. Varadan (Eds.), *Field Representations and Introduction to Scattering*, North-Holland, Amsterdam, 1990, pp. 211–322.
[6] T. Hasegawa, H. Yasutaka, A. Akio, N. Hideki, K. Massahiko, Acoustic radiation pressure acting on spherical and cylindrical shells, *Journal of the Acoustical Society of America* 93 (1993) 154–160.
[7] M.C. Junger, J.M. Garrelick, Short-wavelength backscattering cross sections of rigid and partially coated cylinders and spheres, *Journal of the Acoustical Society of America* 56 (1974) 1347–1353.
[8] A.A. Ferri, J.H. Ginsberg, P.H. Rogers, Scattering of plane wave from submerged object with partially coated surfaces, *Journal of the Acoustical Society of America* 92 (1992) 1721–1728.

[9] C. Partridge, Acoustic scattering from viscoelastically coated bodies, *Journal of the Acoustical Society of America* 99 (1996) 72–78.
[10] F. Honarvar, A.N. Sinclair, Scattering of an obliquely incident plane wave from a circular clad rod, *Journal of the Acoustical Society of America* 102 (1997) 41–48.
[11] J.A. Roumeliotis, N.B. Kakogiannos, Acoustic scattering from an infinite cylinder of small radius coated by a penetrable one, *Journal of the Acoustical Society of America* 97 (1995) 2074–2081.
[12] N.B. Kakogiannos, J.A. Roumeliotis, Acoustic scattering from a sphere of small radius coated by a penetrable one, *Journal of the Acoustical Society of America* 98 (1995) 3508–3515.
[13] Y. Arnaoudov, G. Dassios, V. Kostopoulos, The soft and the hard coated sphere within a point source wave field, *Journal of the Acoustical Society of America* 104 (1998) 1929–1942.
[14] Y. Arnaoudov, G. Dassios, M. Hadjinicloau, The resistive coated sphere in the presence of a point generated wave field, *Mathematical Method in the Applied Sciences* 22 (1999) 73–90.
[15] G. Dassios, M. Hadjinicolaou, G. Kamvyssas, The penetrable coated sphere embedded in a point source excitation field, *Wave Motion* 32 (2000) 319–338.
[16] A.S. Dukhin, P.J. Goetz, T.H. Wines, P. Somasundaran, Acoustic and electroacoustic spectroscopy, *Colloids and Surfaces* 173 (2000) 127–158.
[17] S. Temkin, Attenuation and dispersion of sound in dilute suspensions of spherical particles, *Journal of the Acoustical Society of America* 108 (2000) 126–146.
[18] C.J.T. Sewell, The extinction of sound in a viscous atmosphere by small obstacles of cylindrical and spherical form, *Philosophical Transactions of the Royal Society of London* A210 (1910) 239–270.
[19] W.H. Lin, A.C. Raptis, Acoustic scattering by elastic solid cylinders and spheres in viscous fluids, *Journal of the Acoustical Society of America* 73 (1983) 736–748.
[20] W.H. Lin, A.C. Raptis, Sound scattering from a thin rod in a viscous medium, *Journal of the Acoustical Society of America* 79 (1986) 1693–1700.
[21] T. Hasegawa, Y. Watanabe, Acoustic radiation pressure on an absorbing sphere, *Journal of the Acoustical Society of America* 63 (1978) 1733–1737.
[22] S.M. Hasheminejad, B. Harsini, Effects of dynamic viscoelastic properties on acoustic diffraction by a solid sphere submerged in a viscous fluid, *Archives of Applied Mechanics* 72 (2003) 697–712.
[23] A.S. Dukhin, P.J. Geotz, D.H.M. Simmons, *Ultrasound for Characterizing Colloids*, Elsevier Health Sciences, London, 2002.
[24] R.J. Hill, D.A. Saville, W.B. Russel, Electrophoresis of spherical polymer-coated colloidal particles, *Journal of Colloid and Interface Science* 258 (2003) 56–74.
[25] F. Honarvar, A.N. Sinclair, Nondestructive evaluation of cylindrical components by resonance acoustic spectroscopy, *Ultrasonic* 36 (1998) 845–854.
[26] R.L. Willis, Wu, Lei, Y.H. Berthelot, Determination of the complex young's and shear dynamic moduli of viscoelastic materials, *Journal of the Acoustical Society of America* 109 (2001) 1–11.
[27] M. Giovagnoni, On the direct measurement of the dynamic Poisson's ratio, *Mechanics of Materials* 17 (1994) 33–46.
[28] J. Jarzynski, Mechanisms of sound attenuation in materials, in: R.D. Cosaro, L.H. Sperling (Eds.), *Sound and Vibration Damping with Polymers*, American Chemical Society, Washington DC, 1990, pp. 167–207.
[29] S. Havriliak, S. Negami, A Complex plane analysis of some polymer system, transitions and relaxations in polymers, *Journal of Polymer Science* Part C 14 (1966) 99–117.
[30] B. Hartman, G.F. Lee, J.D. Lee, Loss factor height and width limits for polymer relaxations, *Journal of the Acoustical Society of America* 95 (1994) 226–233.
[31] M. Hasheminejad, T.L. Geers, Modal impedance for two sphere in a thermovicous fluid, *Journal of the Acoustical Society of America* 94 (1993) 2205–2214.
[32] J. Vollmann, J. Dual, High-resolution analysis of the complex wave spectrum in a cylindrical shell containing a viscoelastic medium, Part I. Theory and numerical results, *Journal of the Acoustical Society of America* 102 (1997) 896–908.
[33] J.D. Achenbach, *Wave Propagation in Elastic Solids*, North-Holland, New York, 1976.
[34] P.M. Morse, K.U. Ingard, *Theoretical Acoustics*, McGraw-Hill, New York, 1968.

[35] M. Abramovitz, I.A. Stegun, *Handbook of Mathematical Functions*, National Bureau of Standards, Washington, DC, 1964.
[36] N.B. Vargaftik, *Handbook of Physical Properties of Liquids and Gases*, Springer, Berlin, 1983.
[37] L. Flax, G.C. Gaunaurd, Theory of resonance scattering, in: W.P. Mason, R.N. Thurston (Eds.), *Physical Acoustics*, Academic Press, New York, 1990, pp. 191–294.
[38] Z. Ye, On the low-frequency elastic response of a spherical particle, *Chinese Journal of Physics* 38 (2000) 103–110.
[39] Y.K. Lou, T.C. Su, Free oscillations of submerged spherical shells, *Journal of the Acoustical Society of America* 63 (1978) 1402–1408.
[40] F. Honarvar, A.N. Sinclair, Scattering of an obliquely incident plane wave from a circular clad rod, *Journal of the Acoustical Society of America* 102 (1997) 41–48.
[41] J.C. Piquette, Determination of the complex dynamic bulk modulus of elastomers by inverse scattering, *Journal of the Acoustical Society of America* 77 (1985) 1665–1673.